



Podocyte penetration of the glomerular basement membrane to contact on the mesangial cell at the lesion of mesangial interposition in lupus nephritis: a three-dimensional analysis by serial block-face scanning electron microscopy

Takashi Takaki^{1,2} · Nobuhiko Ohno^{3,4} · Sei Saitoh^{5,6} · Masaaki Nagai⁷ · Kensuke Joh²

Received: 1 October 2018 / Accepted: 19 January 2019 / Published online: 8 February 2019
© Japanese Society of Nephrology 2019

Abstract

Background The interaction among the glomerular components plays an important role in the development of glomerular lesions; thus, investigation of the ultrastructural three-dimensional (3D) configuration of the human glomerular cells and extracellular matrix (ECM) is important for understanding the pathogenesis of glomerulosclerosis, especially glomerulonephritis.

Methods We applied a new technique of serial block-face scanning electron microscopy (SBF-SEM), which helps to acquire serial electron microscopic images to reconstruct a 3D ultrastructure, to a human kidney biopsy specimen obtained from a 25-year-old woman with lupus nephritis.

Results SBF-SEM demonstrated that the cytoplasmic processes of the podocyte penetrated into the lamina densa of the glomerular basement membrane, and was in direct contact with the cytoplasm of mesangial cells at the site of mesangial interposition.

Conclusion Although this is a single-case observational study, SBF-SEM revealed a unique 3D configuration, suggesting a novel mechanism of direct intercellular cross-communication between podocytes and mesangial cells, aside from the presumed paracrine communication.

Keywords Podocyte · Mesangial cell · Glomerular basement membrane · Serial block-face scanning electron microscopy · Renal biopsy · Lupus nephritis

Introduction

The glomerulus is a unique apparatus that filters plasma from blood to urine, and structurally comprises three kinds of proper cells, including endothelial, mesangial,

and epithelial cells (podocyte). The adjacent podocytes are connected by an intercellular junction, which is known as a slit diaphragm, and is separated from endothelial cells by the glomerular basement membrane (GBM) [1]. The fenestrated endothelial cells cover the inner surface of the

✉ Takashi Takaki
takaki@med.showa-u.ac.jp

¹ Division of Electron microscopy, Showa University School of Medicine, 1-5-8 Hatanodai, Shinagawa-ku, Tokyo 142-8555, Japan

² Department of Pathology, Tohoku University Graduate School of Medicine, 2-1 Seiryomachi Aoba-ku, Sendai-shi, Miyagi-ken 980-8575, Japan

³ Division of Histology and Cell Biology, School of Medicine, Jichi Medical University, 3311-1 Yakushiji, Shimotsuke-shi, Tochigi-ken 329-0431, Japan

⁴ Division of Neurobiology and Bioinformatics, National Institute for Physiological Sciences, 5-1 Higashiyama, Myodaiji-cho, Okazaki-shi, Aichi-ken 444-8787, Japan

⁵ Section of Electron Microscopy, Supportive Center for Brain Research, National Institute for Physiological Sciences, Okazaki-shi, Aichi-ken 444-8787, Japan

⁶ Department of Anatomy II and Cell Biology, Fujita Health University School of Medicine, 1-98 Dengakubo, Kutsukake-cho, Toyoake-shi, Aichi-ken 470-1192, Japan

⁷ Division of Nephrology, Narita Memorial Hospital, 134 Haneihonmachi, Toyohashi-shi, Aichi-ken 441-8029, Japan

capillary lumina and are in close contact with mesangial cells in the mesangial area [2, 3]. The three-dimensional (3D) ultrastructural configuration of the glomerular cells and the extracellular components of human glomeruli, especially in glomerulonephritis, is poorly understood. The limited cross-sectional images of the conventional transmission electron microscopy (TEM) cannot easily elucidate the 3D relationships between glomerular cells and the ECM, and can rarely detect the direct cytoplasmic contacts among the glomerular cells. A possible method to solve this problem is multiple serial sectioning of the sample and observation of reconstructed images with TEM, but this process is technically difficult and laborious.

Recently, an automated block-face imaging using scanning electron microscopy, which is called serial block-face scanning electron microscopy (SBF-SEM) [4], has facilitated serial image acquisition and 3D reconstruction of biological materials. In this study, we applied this technique to a human kidney biopsy specimen obtained from a patient with lupus nephritis, and demonstrated a direct cytoplasmic contact between podocytes and mesangial cells, proposing a new idea of podocyte–mesangial cell communication as a mechanism of glomerulosclerosis in human kidney disease.

Materials and methods

Case presentation

A 25-year-old woman presented with bilateral lower limb edema and butterfly rash of the face. Laboratory examination revealed hypoalbuminemia (1.9 g/dL) and massive proteinuria (7.98 g/gCr), which were consistent with nephrotic syndrome. She also presented with microscopic hematuria of 20/hpf; slightly increased serum creatinine (1.39 mg/dL); hypocomplementemia with C3 of 47 mg/dL, C4 of 4 mg/dL, and CH50 of 17 U/mL; a high titer of anti-nuclear antibody at $\times 640$ as a homogenous and speckled pattern; and an increased level of anti-ds-DNA antibody (291 mg/dL). She was diagnosed systemic lupus erythematosus and renal biopsy was performed.

Preparation for light and fluorescent microscopy

The fresh kidney tissue obtained from the renal biopsy was cut into pieces. Some pieces were fixed in 10% formalin/phosphate buffer solution (PBS); embedded in paraffin; sectioned at 2 μm ; and stained with hematoxylin and eosin, periodic acid–Schiff, and Masson trichrome. The other pieces were frozen and stained by the immunofluorescence of human IgG, IgA, IgM, complement 3 (C3), and C1q.

Preparation for transmission electron microscopy

For examination with routine TEM and SBF-SEM, the biopsied sample was pre-fixed in 2.5% glutaraldehyde. For TEM, the tissues were washed four times with PBS for 3 min before incubation with 1% osmium tetroxide for 2 h at 4 °C. After being washed with distilled water for 5 min, the tissues were dehydrated and placed in propylene oxide twice for 10 min; a 1:3 mixture of resin and propylene oxide; a 1:1 mixture of resin and propylene oxide; a 3:1 mixture of resin and propylene oxide; and, finally, 100% resin. The resins were prepared from the Quetol 812 kit (Quetol 812 9.7 mL, DDSA 3.3 mL, MNA 6.6 mL, and DMP-30 0.3 ml for 20 mL) and were cured at 60 °C for 3 days. The sample was sliced at 70 nm using an ultramicrotome (Ultracut-UCT, Leica). After staining of the ultrathin sections with uranyl acetate and lead citrate, TEM observation was performed using JEM-1400 (JEOL Ltd.).

Preparation for serial block-face scanning electron microscopy

To examine the 3D architecture of the glomerular cells and ECM, serial image acquisitions and 3D reconstruction of the kidney biopsy sample were performed by SBF-SEM, as described previously [5, 6]. Briefly, the tissues were fixed in 2.5% glutaraldehyde and were washed four times with PBS for 3 min and then incubated with 2% OsO₄ in 1.5% potassium ferrocyanide for 20 min at room temperature (RT). After being washed with distilled water, the tissues were incubated in filtered thiocarbonylhydrazide solution for 20 min at RT. After washing again with distilled water, the tissues were incubated in a newly prepared 2% OsO₄ for 30 min at RT. The tissues were placed in lead aspartate solution and then returned to an oven at 60 °C for 30 min. The tissues were dehydrated in a graded series of ethanol (60%, 80%, 90%, and 95% for 5 min each), followed by infiltration with acetone that was dehydrated with a molecular sieve; a 1:1 mixture of resin and acetone; and 100% resin. The resins were prepared from the Quetol 812 kit in the same manner as that for the TEM preparation; 7% Ketjen black was added to increase the conductivity of the resin. The surfaces of the trimmed samples were treated with gold sputtering to increase conductivity and imaged on field emission-SEM (Merlin or Sigma, Carl Zeiss AG.) equipped with 3View (Gatan, Inc.). The obtained serial images were handled with ImageJ with Fiji plugins (<http://fiji.sc/>). Segmentation and image analyses were performed with the software of Microscopy Image Browser (<http://mib.helsinki.fi.>) [7] and Amira (FEI Visualization Science Group, Hillsboro, OR, USA).

Results

Pathological findings on light and fluorescent microscopy

The kidney tissue contained a total of 18 glomeruli, which comprised 1 global sclerosis, 4 cellular crescents, 3 fibrocellular crescents, and 1 fibrous crescent (Fig. 1a). The non-sclerotic glomeruli had diffuse mesangial and endocapillary hypercellularity with neutrophilic infiltration, as well as focal and segmental mesangial interposition (Fig. 1b). Immunofluorescence showed diffuse and global fine granular deposits of IgG (+), IgA (+), IgM (+), C3 (2+), and C1q (+) in the mesangial area and glomerular capillary walls (Fig. 1c). The pathological diagnosis was lupus nephritis, class IV-G (A/C), based on the International Society of Nephrology/Renal Pathology Society classification.

3D ultrastructural configuration of the glomerular lesion on SBF-SEM

We took 250 serial images of SBF-SEM; segmentation and analyses were performed on 225 of these images. We focused on one glomerular capillary and paramesangial area,

which showed mesangial interposition containing a capillary lumen on the 48th image (Fig. 2a). The glomerulus comprised interwoven capillary loops and the endothelial cells were lined in yellow along the GBM (Fig. 2b). The podocytes were located above the GBM, whereas the mesangial cells were located beneath the lamina densa of the GBM. The foot processes of the podocytes above the GBM showed segmental effacement (Fig. 2a, c). On the 110th image of the same capillary tuft, disruption of the GBM by podocytic cytoplasmic processes was observed (Fig. 2c, d). In this image, the glomerular capillary lumen was not recognized; therefore, the cells located beneath the GBM were considered as mesangial cells at the mesangial interposition (Fig. 2d). To obtain highly magnified configurations of the disrupted GBM and the podocytic cytoplasmic processes, we selected an area and followed 225 serial sections of 80-nm thickness and reconstructed a 3D image of the area of interest (18- μ m specimen thickness) (Fig. 3a). Disruption of the GBM was observed on the 110th section, although the GBM was continuous on the 88th and 115th sections (Fig. 3b). In the same sections, the GBM matrix was segmented as green, showing the disruption on the 110th section (Fig. 3c).

We reconstructed a 3D image using these serial sections that showed the podocyte cytoplasmic process (Fig. 4a). The cytoplasmic processes of the podocyte infolded deeply into

Fig. 1 Light microscopy examination of the biopsied kidney tissue. **a** At a lower magnification of a paraffin section stained with Masson trichrome, some glomeruli exhibit a cellular crescent (arrowhead) and fibrinoid necrosis in an afferent artery is observed (arrow). **b** At a higher magnification of a paraffin section stained with periodic acid–Schiff, the glomeruli have diffuse mesangial proliferation with endocapillary hypercellularity (arrowheads). **c** Immunofluorescence shows diffuse and global fine granular deposits of IgG, IgA, IgM, C3, and C1q in the mesangial area and glomerular capillary walls

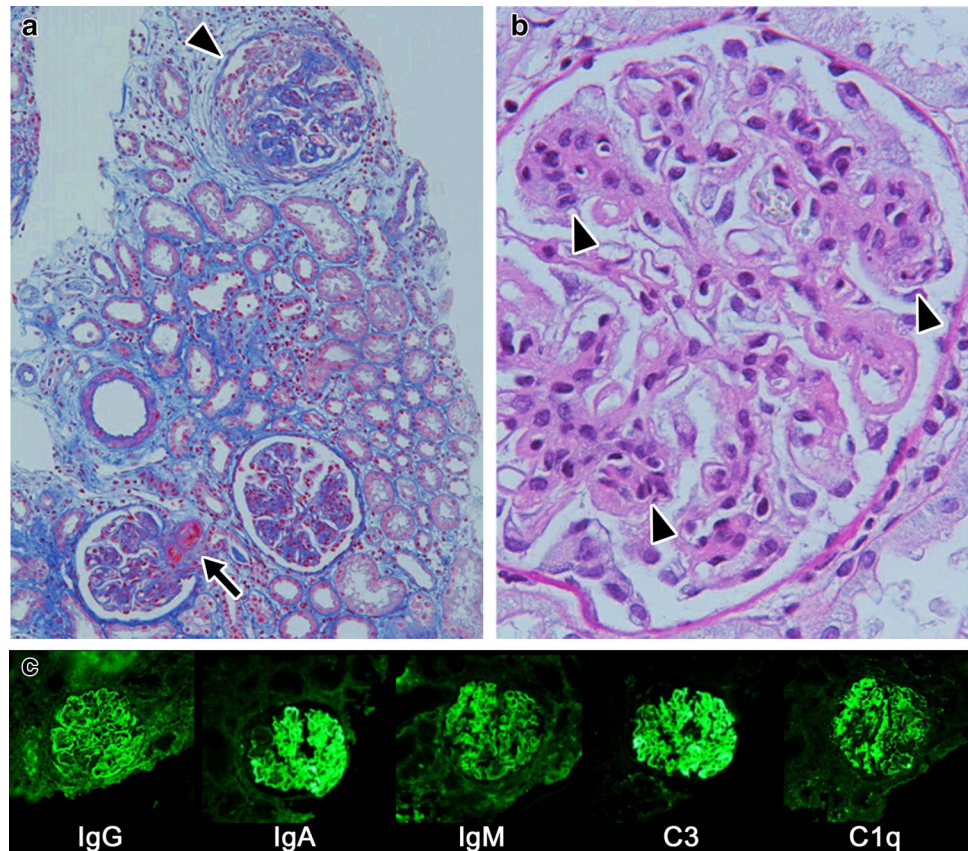
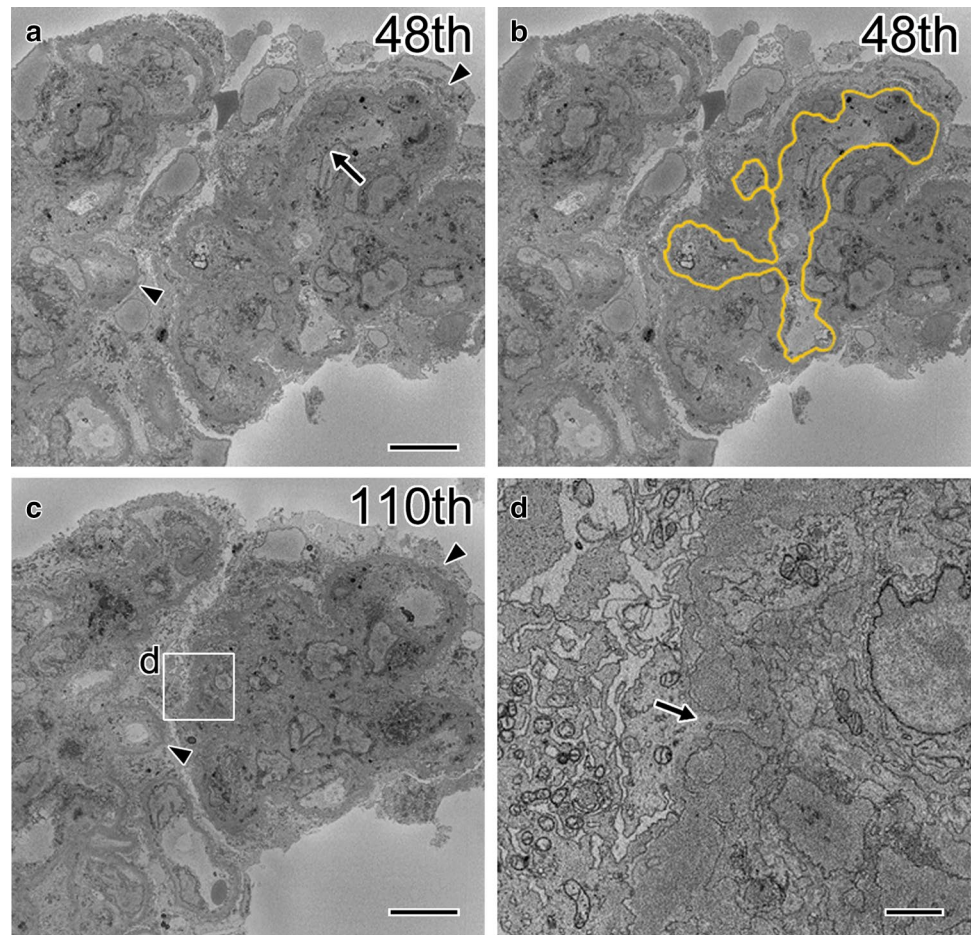


Fig. 2 Disruption of the GBM with a penetrating podocyte cytoplasmic process at the mesangial interposition on serial images obtained by SBF-SEM at a lower magnification. **a** The 48th section shows mesangial interposition (arrow) containing a capillary lumen. **b** The basal side of the endothelial cells facing the GBM is lined in yellow along the contour of the glomerular capillary. **a, c** The foot processes of podocytes above the GBM show segmental effacement (arrowheads). **c** The 110th section of the same capillary tuft shows mesangial interposition without a capillary lumen. The region indicated by a white square in (c) is magnified in (d). **d** Disruption of the GBM with a penetrating podocyte cytoplasmic process (arrow) is demonstrated in the 110th section. Bars: 10 μm (a, b) and 2 μm (c)



the GBM and extended into the mesangial matrix that surrounded the mesangial cells (Fig. 4a). At an arbitrary site where the podocyte was found to penetrate most into the mesangial area, the invading podocyte was seen to come close to the cytoplasm of the mesangial cell (Fig. 3b). At higher magnification, the podocyte cytoplasmic process was seen to be in direct contact with the cytoplasm of the mesangial cell (Fig. 3b, c). A dense patch was observed beneath the cytoplasmic membrane of the cell located in mesangial matrix, indicating an evidence of mesangial cell origin (Fig. 3b, d). The areas of contact between the podocyte cytoplasmic processes and the mesangial cells were not broad but pin-pointed (Fig. 4c, d).

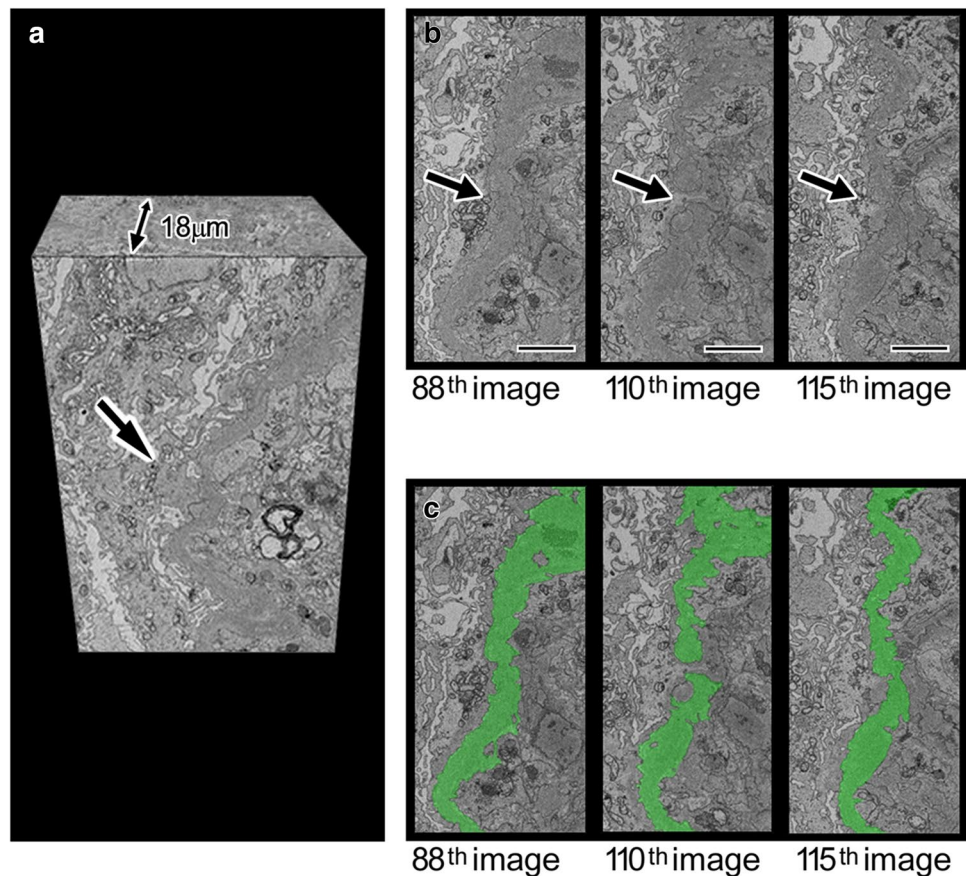
To demonstrate the distribution of the direct contact between the podocytes and mesangial cells, 3D reconstruction of the podocyte cytoplasm and the mesangial cells was made, excluding the mesangial matrix to avoid obscure imaging of the contact sites (Fig. 5a). The podocyte cytoplasmic process invading the mesangial matrix had many spikes directed toward the mesangial cells; the sites of contact with the mesangial cells were also indicated (Fig. 5a). Attached to the mesangial cells were 110 spikes, which represented the points of contact in a tissue volume of 3,700

μm^3 (Fig. 5a, b). One podocyte was in contact with seven mesangial cells, although the cell margins are not represented in Fig. 5a.

Comparison of TEM and SBF-SEM images as a diagnostic tool for kidney biopsy

To evaluate the diagnostic potential of the SBF-SEM method, we compared the obtained electron microscopic images between SBF-SEM and conventional TEM. A rapid tissue preparation method using a combination of reduced osmium, thiocarbohydrazide, and osmium (r-OTO method) in SBF-SEM increased the contrast of the cytoplasmic and nuclear membranes of the glomerular cells, thereby making the cellular and nuclear shapes relatively clear in the images obtained by SBF-SEM, even without uranyl acetate staining [5, 6]. Therefore, the podocytes, endothelial cells, and mesangial cells in the glomeruli were clearly observed by SBF-SEM (Fig. 6b, d), as well as by TEM (Fig. 6a, c). However, density and contrast of the GBM and mesangial matrix were lower in the SBF-SEM images than in the TEM images. In addition, the immune deposits observed in the subendothelial and paramesangial areas showed lower

Fig. 3 Disruption of the GBM with penetrating podocyte processes, as observed on SBF-SEM at a higher magnification. **a** Reconstructed three-dimensional images (18- μ m specimen thickness) of the examined area through 225 serial sections at 80-nm thickness each. **b** Disruption of the GBM is observed on the 110th section, but the GBM is continuous on the 88th and 115th sections. **c** The GBM matrix is segmented as green, showing the disruption on the 110th section. Bars: 2 μ m



density in SBF-SEM images (Fig. 6b, d) than in the conventional TEM images (Fig. 6a, c). Nuclear chromatin density (heterochromatin) was lower in SBF-SEM than in TEM.

Discussion

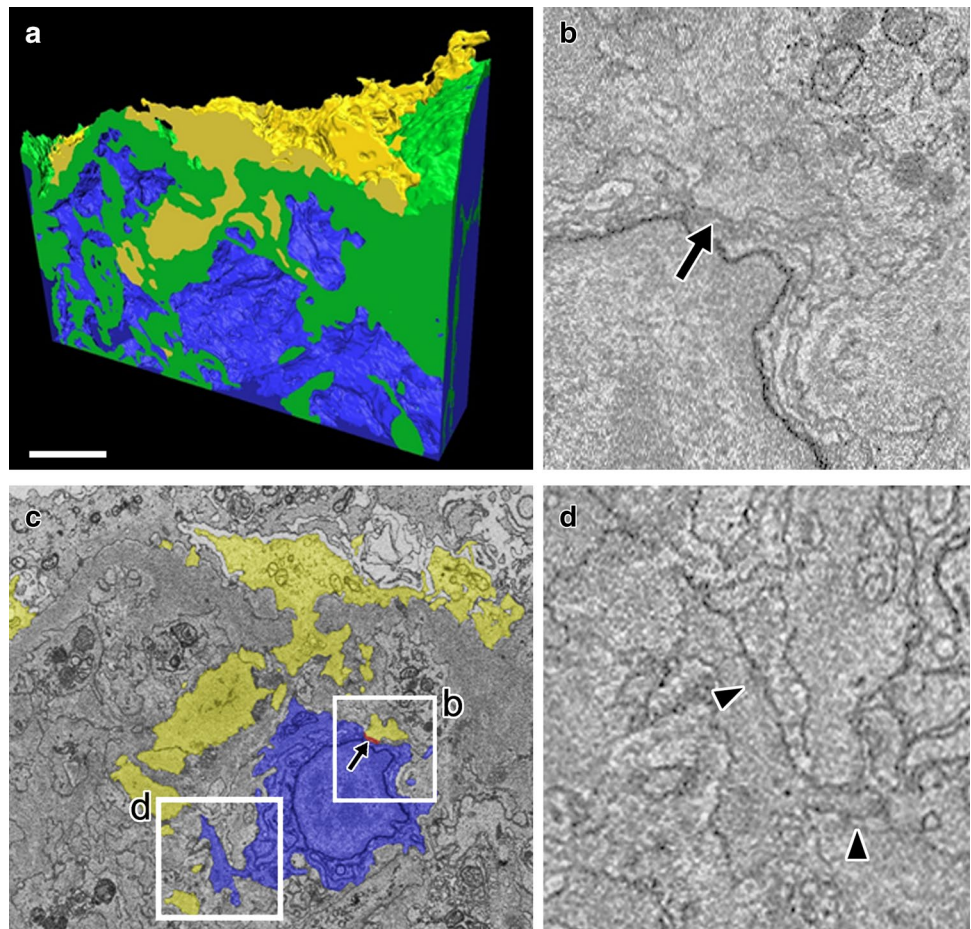
To our knowledge, this is the first study examining human kidney tissue with SBF-SEM. We examined the biopsy specimen of human lupus nephritis to demonstrate the ultrastructural relationship between podocytes and mesangial cells. By SBF-SEM, we tracked the cytoplasmic processes of the podocyte, which infolded into the GBM and penetrated into the subendothelial area with mesangial interposition and formed multiple direct cytoplasmic connections with the cytoplasm of the mesangial cells.

Since we started this SBF-SEM analysis focusing on the direct cellular interactions in the glomerular diseases, we have collected 14 renal biopsy specimens, including cases of lupus nephritis, IgA nephropathy, diabetic glomerulopathy, and benign nephrosclerosis. To observe a direct cellular communication among epithelial, endothelial, and mesangial cells in the glomeruli, we selected the cases accompanying mesangial interposition, a severe form of glomerular inflammation, where the cell proliferation and disruption of GBM

were considered to occur frequently. The present case was the first where the remarkable penetration of the podocytic cytoplasm into the GBM contacting on mesangial cell at the lesion of mesangial interposition was found. Thereafter, we found a similar podocyte–mesangial cell communication in an IgA nephropathy case (manuscript in preparation). Thus, we speculate that this unique phenomenon of podocyte–mesangial cell contact is not an incidental finding in a single case of lupus nephritis but a more usual and common feature of podocyte behavior under severe glomerular inflammation that could be observed in different types of glomerular diseases. A direct evidence on the cross-communication between podocytes and mesangial cells was scarcely reported in the literature [8, 9]. Although the exact role of a podocyte–mesangial cell interaction has not been analyzed *in vitro*, the observation of a direct contact between these cells provides a new insight into glomerular inflammation mechanism where intrinsic glomerular cells physically interact with each other. Further study using samples from different glomerular diseases is needed to understand the association of this finding with the pathophysiology of glomerular diseases.

How the podocyte cytoplasmic processes penetrate through the GBM to reach the mesangial cells and matrix remains to be elucidated. Possibly, cytoplasmic processes

Fig. 4 Direct contact of the podocyte cytoplasmic processes with the mesangial cells. **a** Three-dimensional reconstruction of serial sections shows deep infolding of the podocyte cytoplasmic process (yellow) into the GBM and the mesangial matrix (green) that surrounds the mesangial cells (blue). Bar: 5 μ m. **c** At a lower magnification, the podocyte (yellow) is seen to penetrate through the GBM into the subendothelial matrix and to come close to the cytoplasm of the mesangial cell (blue arrow). The areas indicated by the white squares are magnified (**b**, **d**). **b** At a higher magnification, the podocyte cytoplasmic process is seen to be in direct contact with the cytoplasm of the mesangial cell (arrow). **d** A dense patch is observed beneath the cytoplasmic membrane of the mesangial cell, indicating evidence of mesangial cell origin (arrow). The contact areas are not sheet-like but, rather, punctate contacts between the cytoplasmic processes of both the podocyte and mesangial cells



passively translocate into the mesangial space as a result of GBM disruption. Another possibility is that they may actively disrupt GBM and migrate into the mesangial space. Similar podocyte behavior has been observed in some cases of membranous nephropathy, and this phenomenon has been reported as a new disease entity, podocytic infolding glomerulopathy [10]. Although whether podocytic infolding is a specific finding of this distinct disease entity remains debatable, podocytes can sneak into GBM under the circumstances of glomerular inflammation. This type of podocytic infolding has been usually localized in the region of GBM and rarely penetrates into the mesangium. Conversely, in the present case, podocytes penetrated into the mesangium at the mesangial interposition. We speculate this phenomenon as a type of repair process after GBM and mesangial matrix disruption. When GBM is disrupted due to causes such as mechanical, chemical, or inflammatory cellular injury, podocytes attempt to repair the disrupted area by invading into the mesangial matrix. The podocytes sneaking into the mesangium may eventually come in contact with mesangial cells, which may stimulate their cellular responses to each other, thus, promoting the repair processes. These speculations must be investigated further using *in vitro* and *in vivo*

experimental models mimicking the glomerular injury and repair processes.

The interactions among the glomerular cells are usually achieved by paracrine signaling [3, 9]. The vascular endothelial growth factor (VEGF)-A produced by podocytes regulates the structure and function of adjacent endothelial cells via VEGF receptor 2, which are expressed in the endothelial cells of both the developing and mature adult kidneys [8, 11–13]. The cross-communication between glomerular endothelial cells and the nearby mesangial cells may be mediated by platelet-derived growth factor (PDGF)-B signaling. The endothelial cells produce PDGF-B, and the PDGF receptor B (PDGFR-B) is expressed in mesangial cells [3]. Therefore, in the paracrine cross-communication among glomerular cells, podocytes may affect the endothelial cells via VEGF-A, and endothelial cells may communicate with the mesangial cells via PDGF-B [14, 15].

The SBF-SEM, a novel innovated technology, enables the rapid observation of the 3D ultrastructure of a large number of biological specimens. In this method, the specimen is automatically cut by an ultramicrotome that is equipped in the SEM chamber, and images are observed by backscattered electron (BSE). The merits of this method are automated

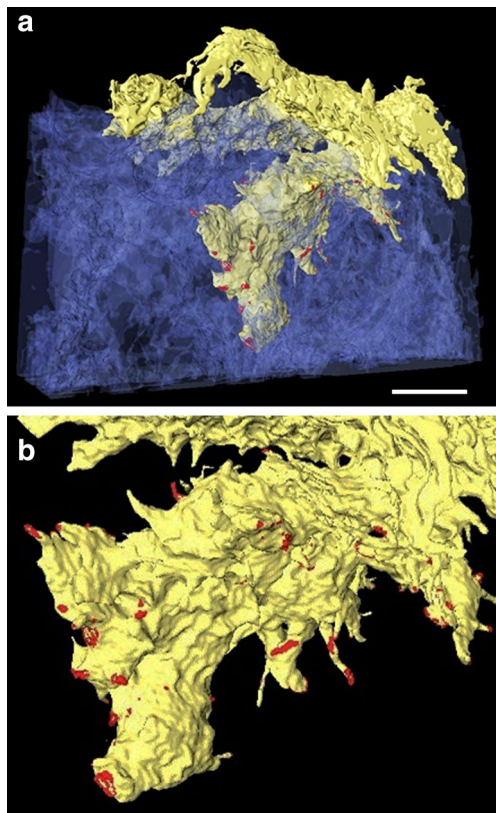


Fig. 5 Three-dimensional configuration of the podocyte and its contact with the mesangial cells. **a** The podocyte cytoplasmic process invading into the mesangial matrix has several spikes (yellow) approaching the mesangial cells (blue), and the sites of contact (red) with the mesangial cells are indicated. Bar: 5 μm . **b** Higher magnification of the cytoplasmic process shows 110 points of contact (red) between the podocyte and the mesangial cells in a tissue specimen with a volume of 3700 μm^3

multi-sectioning of the sample and serial observation to construct the 3D image. This approach was recently used to investigate the cell–ECM interactions in a murine lupus nephritis model [6] and the complex podocyte structures in an experimental model of Alport syndrome [9]. Other recent techniques, such as focused ion beam SEM (FIB-SEM) and automated tape-collecting ultramicrotome SEM (ATUM-SEM), were also reported to enable 3D reconstruction at a subcellular resolution that was similar to that of the SBF-SEM method [5, 6]. In FIB-SEM, gallium ion beam, instead of the ultramicrotome, is used to obtain multiple serial surfaces of the sample and the images are observed

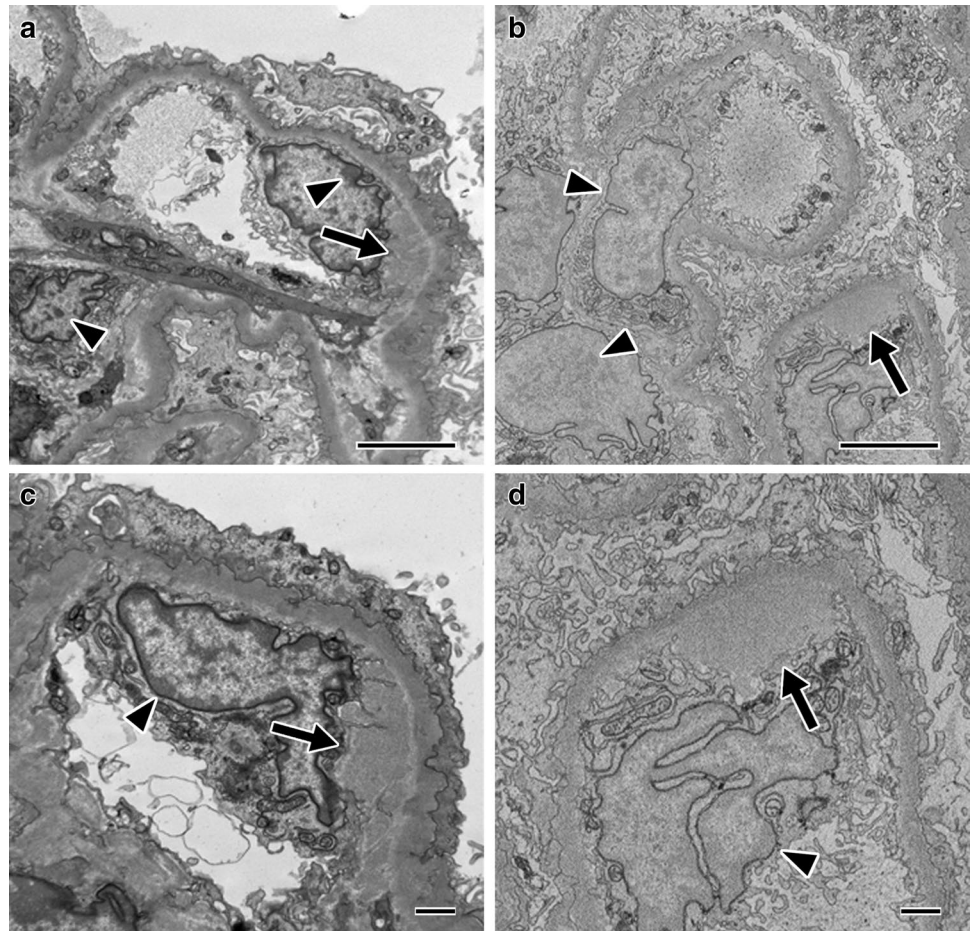
by BSE, as with SBF-SEM. Compared with SBF-SEM, the FIB-SEM can likewise gain the multiple serial images easily, but the observed area is smaller because of the limited field of ion beam emission. In ATUM-SEM, multiple serial ultrathin sections of the sample are cut by the conventional ultramicrotome, mounted on a silicon plate in array, and observed by SEM using BSE. This method is very laborious and requires a high skill to obtain multiple serial ultrathin sections, but it has the advantage of not requiring a special equipment that is used in SBF-SEM and FIB-SEM [16]. Considering the characteristics of these methods, we need to select the appropriate method according to the kind of sample and the purpose of the research. Although we utilize these methods, the most serious problems of 3D image analysis are the huge amount of data and the laborious segmentation of the obtained figures. Segmentation is the step to distinguish the contour of the cell or structure by color in the serial images and cannot be performed automatically. Innovated technology, such as deep learning or artificial intelligence, may be required to overcome this limitation of 3D imaging.

In this study, application of an additional en-bloc staining with lead aspartate solution and the r-OTO method before embedding generated SBF-SEM images that were almost comparable with those obtained by the conventional TEM. The reason for the low electron density and low contrast of the images obtained by SBF-SEM was probably the lack of uranyl acetate in the post-fixed staining in our present procedure. By obtaining the morphologic alterations in glomerular diseases, a simplified preparation method for SBF-SEM can replace the usual complicated preparation methods for TEM for routine diagnosis. The current staining methods for SEM, along with additional heavy metal staining, will be useful for clinical application and diagnostic pathology.

Limitation of this study

This is a single-case study using one biopsy sample. Thus, the significance of the findings observed in the 3D reconstruction images in this case should be investigated using multiple samples obtained from patients with similar and different glomerular diseases. Therefore, the conclusion is speculative and difficult to define under these limited circumstances.

Fig. 6 Comparison of the conventional TEM and SBF-SEM images. The conventional TEM images in low (a) and high (c) magnification show distinct contours of the glomerular cells, and electron staining with uranyl acetate and lead citrate clearly shows electron-dense deposits (EDD) in the subendothelial and paramesangial areas (arrows) and nuclear heterochromatin (arrowheads). SBF-SEM images in low (b) and high magnification (d) show relatively clear cellular and nuclear membranes but lower density of the GBM, mesangial matrix, and EDD. Compared with the images obtained by conventional TEM, these SBF-SEM images show relatively difficult recognition of the EDD (arrow) and obscure nuclear heterochromatin (arrowheads). Bars: 4 μm (a, b) and 1 μm (c, d)



Acknowledgements We thank Professor Kazuho Honda of the Department of Anatomy, Showa University School of Medicine for the critical reading and helpful suggestions; Drs. Truc Quynh Thai and Huy Bang Nguyen of the Division of Neurobiology and Bioinformatics, National Institute for Physiological Sciences, Okazaki, Japan for providing technical assistance; and Ms. Atsuko Imai of the Division of Cell Structure, National Institute for Physiological Sciences, Okazaki, Japan for her kind support in the segmentation and 3D techniques. The authors would like to thank Enago (<http://www.enago.jp>) for the English language review.

Author contributions MN was the attending physician of the patient. KJ, NO, and TT wrote the manuscript. NO, SS, and TT performed the genetic analyses. TT performed the observation with the TEM. NO, SS, and TT performed the observation with the SBF-SEM. KJ is a renal pathologist who helped diagnose the patient. All authors read and approved the final manuscript.

Funding This work was partly supported by the JSPS KAKENHI Grant (number 26460449) to KJ; the Cooperative Research Program of Network Joint Research Center for Materials and Devices granted to KJ, MN, and TT; and a Grant-in-Aid for Scientific Research on Innovative Areas-Resource and technical support platforms for promoting

research of Advanced Bioimaging Support (JP16H06280) to KJ, MN, and TT.

Compliance with ethical standards

Ethical approval All procedures that involved human participants were performed in accordance with the ethical standards of the institution at which the study was conducted (IRB approval number 2015-1-514, Tohoku University School of Medicine) and with the 1964 Helsinki Declaration and its later amendments or comparable ethical standards.

Conflict of interest The authors have declared that no conflict of interest exists.

Informed consent Informed consent was obtained from all participants in the study.

Consent for publication The patient gave informed consent for data publication.

References

1. Pavenstadt H, Kriz W, Kretzler M. Cell biology of the glomerular podocyte. *Physiol Rev.* 2003;83:253–307.
2. Mene P, Simonson MS, Dunn MJ. Physiology of the mesangial cell. *Physiol Rev.* 1989;69:1347–424.
3. Schlondorff D, Banas B. The mesangial cell revisited: no cell is an island. *J Am Soc Nephrol.* 2009;20:1179–87.
4. Ohno N, Katoh M, Saitoh Y, Saitoh S, Ohno S. Three-dimensional volume imaging with electron microscopy toward connectome. *Microscopy (Oxf).* 2015;64:17–26.
5. Nguyen HB, Thai TQ, Saitoh S, Wu B, Saitoh Y, Shimo S, Fujitani H, Otobe H, Ohno N. Conductive resins improve charging and resolution of acquired images in electron microscopic volume imaging. *Sci Rep.* 2016;6:23721.
6. Thai TQ, Nguyen HB, Saitoh S, Wu B, Saitoh Y, Shimo S, Elewa YH, Ichii O, Kon Y, Takaki T, Joh K, Ohno N. Rapid specimen preparation to improve the throughput of electron microscopic volume imaging for three-dimensional analyses of subcellular ultrastructures with serial block-face scanning electron microscopy. *Med Mol Morphol.* 2016;49:154–62.
7. Cocks E, Taggart M, Rind FC, White K, Amira. A guide to analysis and reconstruction of serial block face scanning electron microscopy data. *J Microsc.* 2018; 1365–2818.
8. Dimke H, Maezawa Y, Quaggin SE. Crosstalk in glomerular injury and repair. *Curr Opin Nephrol Hypertens.* 2015;24:231–8.
9. Randles MJ, Collinson S, Starborg T, Mironov A, Krendel M, Konigshausen E, Sellin L, Roberts IS, Kadler KE, Miner JH, Lennon R. Three-dimensional electron microscopy reveals the evolution of glomerular barrier injury. *Sci Rep.* 2016;6:35068.
10. Joh K, Taguchi T, Shigematsu H, et al. Proposal of podocytic infolding glomerulopathy as a new disease entity: a review of 25 cases from nationwide research in Japan. *Clin Exp Nephrol.* 2008;12:421–31.
11. Bertuccio C, Veron D, Aggarwal PK, Holzman L, Tufro A. Vascular endothelial growth factor receptor 2 direct interaction with nephrin links VEGF-A signals to actin in kidney podocytes. *J Biol Chem.* 2011;286:39933–44.
12. Sison K, Eremina V, Baelde H, Min W, Hirashima M, Fantus IG, Quaggin SE. Glomerular structure and function require paracrine, not autocrine, VEGF-VEGFR-2 signaling. *J Am Soc Nephrol.* 2010;21:1691–701.
13. Dimke H, Sparks MA, Thomson BR, Frische S, Coffman TM, Quaggin SE. Tubulovascular cross-talk by vascular endothelial growth factor a maintains peritubular microvasculature in kidney. *J Am Soc Nephrol.* 2014;26:1027–38.
14. Eremina V, Sood M, Haigh J, Nagy A, Lajoie G, Ferrara N, Gerber HP, Kikkawa Y, Miner JH, Quaggin SE. Glomerular-specific alterations of VEGF-A expression lead to distinct congenital and acquired renal diseases. *J Clin Invest.* 2003;111:707–16.
15. Floege J, Eitner F, Alpers CE. A new look at platelet-derived growth factor in renal disease. *J Am Soc Nephrol.* 2008;19:12–23.
16. Titze B, Christel Genoud. Volume scanning electron microscopy for imaging biological ultrastructure. *Biol Cell.* 2016;108:307–23.

Publisher's Note Springer Nature remains neutral with regard to jurisdictional claims in published maps and institutional affiliations.